MATHEMATICAL MODELLING OF WELD PHENOMENA 12

Edited by
C. Sommitsch
N. Enzinger
P. Mayr

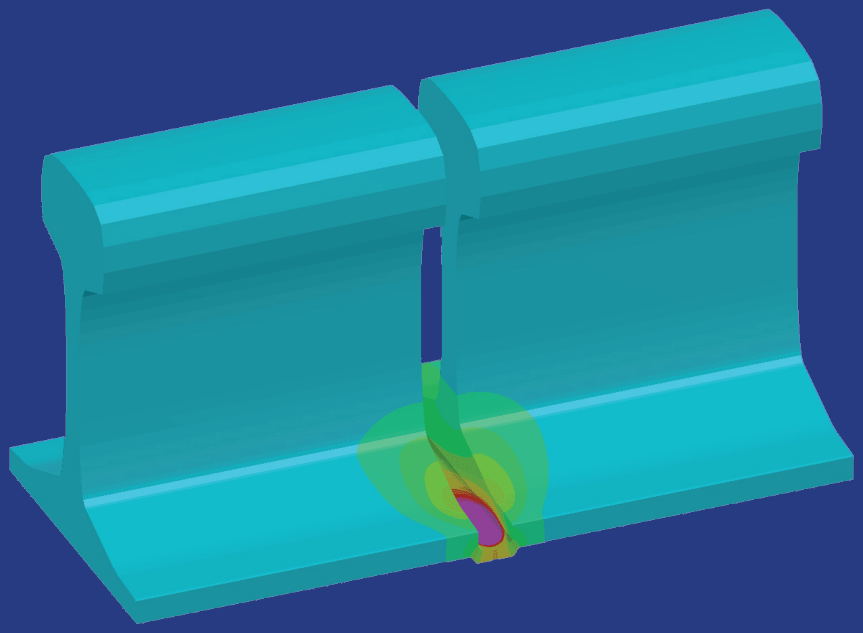

SIMULATION OF WELDING RESIDUAL STRESSES – FROM THEORY TO PRACTICE

S. GKATZOGIANNIS*, P. KNOEDEL* and T. UMMENHOFER*

*Karlsruhe Institute of Technology, KIT Steel & Lightweight Structures - Research Center for Steel, Timber & Masonry, Otto-Ammann-Platz 1, 76131, Karlsruhe, Germany, stefanos.gkatzogiannis@kit.edu

DOI 10.3217/978-3-85125-615-4-21

ABSTRACT

The present study reviews previous and new simulations of welding residual stresses with the finite element method. The influence of modelling mechanical boundary conditions, erroneous prediction of the weld heat source coefficient, the influence of microstructural changes in aluminium welds and the consideration of strain-rate sensitivity of steel are investigated. The results are analysed so that sound conclusions regarding the investigated factors, acting as recommendations for the practitioner, can be presented.

Keywords: Weld simulation, strain-rate dependency, boundary conditions, heat input, aluminum welding

List of Notations

f_r	heat fraction deposited in the rear quadrant of Goldak's heat source (J)
f_f	heat fraction deposited in the front quadrant of Goldak's heat source (J)
Q	thermal power or energy input rate (Watt or J/s)
C	characteristic radius of flux distribution (m)
v	welding source travel (m/s)
t	time (s)
τ	lag factor ("phase shift") needed to define the position of weld heat source source at time t = 0
V	voltage (V)
I	current of the weld metal arc (A)
η	weld metal arc efficiency (-)
ρ	density (Kg/m^3)
c	specific heat (J/(kg K))
T	temperature (K)
K_{xx}, K_{yy}, K_{zz}	thermal conductivity in the element's x, y, and z directions (W/(m K))
$\dot{Q}$	heat generation rate per unit volume (W/m^3)
α^{se}	temperature dependent coefficient of thermal expansion
T_{ref}	reference temperature for thermal strains (°C)
$f_s(u)$	resisting force as a function of deformation (N)
p(t)	external transient loading (N)

E	Young's modulus (N/mm^2)
v	Poisson's ratio (-)
σ_ε	the von Misses effective stress (N/mm^2)
$\dot{\hat{\varepsilon}}_{pl}$	equivalent plastic strain rate (-)
σ	yield stress at the investigated strain rate (N/mm^2)
σ_o	static yield stress (N/mm^2)
γ and m	coefficients with no direct physical meaning characterizing the strain rate hardening behavior

INTRODUCTION

The mathematical background for modelling welding phenomena exists since the 80's [1]. Simple FE models for academic purpose have been developed ever since [2]. Nevertheless, the increase of computational power during the last 2 decades allowed the creation of more sophisticated three-dimensional models for practical applications as well ([3], [4], [5], [6] etc.). This rapid increase in applications regarding weld simulation did not allow detailed documentation of the applied approaches. Despite the thorough existing theoretical background, the lack of established practical methods is profound.

Main interest of industrial applications lies in the calculation of welding residual stresses (WRS) and distortions with high preciseness but reduced computational effort [8]. For this purpose, an engineering approach, which is applicable to any commercial general purpose FE Software, takes into consideration microstructural changes and can be reproduced by a non-metallurgist for modelling various alloys requiring only basic knowledge of material science, was proposed in previous work by the authors of the present paper [3]. Use of this method, which was validated for single-pass welds, has enabled the investigation of factors, which influence significantly the simulated welding residual stresses, in all three fields of weld simulation: the thermal, the microstructural and the mechanical field.

Previous work of the authors has highlighted the significant practical aspects and the predominant factors of weld simulation that influence the calculated welding residual stresses. A review of this previous work, regarding the influence of mechanical boundary conditions [9], material models [10], [11], heat input parameters [12], along with new series of analyses regarding the influence of microstructural transformation in the case of aluminium welding, are presented in the current paper. Moreover, the background for an extension of the previously presented model [3] to multi-pass welds is outlined. The conclusions can work as a guide for the practitioner, in order to exclude effects during modelling and decrease in extension the computational effort, without reducing the required accuracy from an engineering point of view.

THEORETICAL BACKGROUND

MODELLING OF WELDING RESIDUAL STRESSES AND DISTORTION

Welding is a multiphysics problem, but simulation of WRS requires modelling only of some aspects of the welding process. The thermal behavior and possible microstructural changes are investigated along with the mechanical behavior of a component when WRS are under the scope. These three fields, which are presented in Fig. 1 are interacting bidirectionally with each other. Practical models, predicting the WRS with satisfying preciseness by only simulating the interaction of thermal on microstructural and mechanical behavior and of microstructural field on the mechanical behavior have been suggested [8] and developed [3]. The considered interactions are presented in Fig. 1. Ignoring the reverse influence of microstructural and mechanical behavior enables solution of the problem with a sequential unidirectionally coupled thermal–mechanical analysis [3].

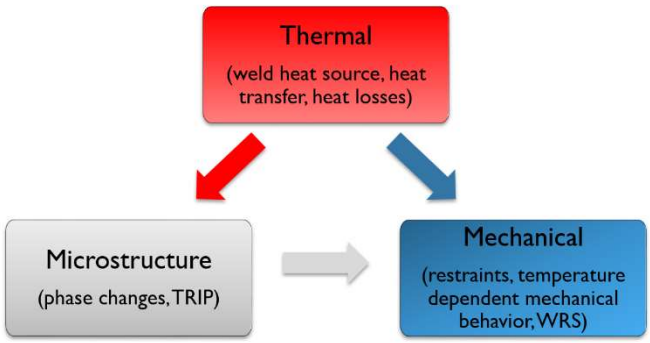

Fig. 1 Investigated fields and respective interactions in an engineering approach for arc welding simulation, TRIP stands for transformed induced plasticity [3]

Thermal modelling

Thermal modelling tackles the problem of heat transfer. Simulation of the heat transfer inside the investigated component, the weld heat source and heat losses to the surrounding environment (boundary conditions) is required in this filed. According to Goldak's double ellipsoidal model, which is the state-of-the-art approach for modelling the weld heat source [13], the power density distribution inside front and rear quadrant are described by the following two equations respectively (Eqn. (1) and (2)):

$$q(x,y,z,t)=\frac{6\sqrt{3}f_f Q}{abc\pi\sqrt{\pi}}e^{-3x^2/a^2}e^{-3y^2/b^2}e^{-3[z+v(\tau-t)]^2/c^2} \quad (1)$$

and

$$q(x,y,z,t)=\frac{6\sqrt{3}f_rQ}{abc\pi\sqrt{\pi}}e^{-3x^2/a^2}e^{-3y^2/b^2}e^{-3[z+v(\tau-t)]^2/c^2}. \quad (2)$$

The effective energy input rate (thermal power, equal to the electric power of the arc minus the losses) is predicted according to the following Eqn. (3) [3]

$$Q=\eta VI\ . \quad (3)$$

Heat input h is calculated by dividing Eqn. (3) with the welding speed. Proposed values for the η coefficient for various weld types are proposed in [14]. Nevertheless, different values usually in a range of ±10 % for same welding types are found elsewhere (see [2] etc.). Combining the first thermodynamics law (conservation of energy) with Fourier's law for heat conduction and neglecting the fluid flow in the weld pool, the transient heat transfer Eqn. (4) which governs the heat transfer inside the component is calculated [15]:

$$\rho c\frac{\partial T}{\partial t}=\dot{Q}_G+\frac{\partial}{\partial x}\left(Kx\frac{\partial T}{\partial x}\right)+\frac{\partial}{\partial y}\left(Ky\frac{\partial T}{\partial y}\right)+\frac{\partial}{\partial z}\left(Kz\frac{\partial T}{\partial z}\right). \quad (4)$$

Heat losses are modelled according to Newton's law of cooling (Eqn. (5))

$$\frac{q}{A}=h_f(T_s-T_b)\,. \quad (5)$$

A transient thermal analysis is carried out, whereby the temperature history of the nodes of the FE model are saved at each solution step.

Microstructural modelling

Various models have been proposed in the past, in order to predict the metallurgical transformations during a weld thermal cycle ([16], [17] etc.). A straightforward engineering approach, which was proposed by the authors of the present study [3], provided results with sufficient preciseness. The method is applicable for the simulation of various materials [9], [12], [10]. Main feature of the approach lies on the assignment of material models to the finite elements inside the fusion zone (FZ) and the heat-affected zone (HAZ) during cooling down based on predominant parameters of the thermal cycle, in order to simulate the modified mechanical behavior of the transformed microstructure. The considered parameters are the the maximum reached temperature inside a thermal cycle T_{max}, the time needed for the temperature to drop from 800 °C to 500 °C during cooling down inside a thermal cycle t_{85}, and the austenitization time t_a, during which the temperature is above the austenitization temperature (Ac1) inside a thermal cycle.

In the case of single-pass butt-welds the austinetization time is similar in all areas around the weld [2], [3]. Austinetization time influences the proportion of the parent material, which is transformed to austenite during warm up and is subsequent to metallurgical transformations during cooling down. This proportion is as well influenced by the

maximum achieved temperature. The coupled influence of these two parameters on the proportion of the austenitized temperature, can be expressed only by the T_{max}, if the retardation effect is taken into consideration. When high heating rates and thus, short austenitization times, are present the temperature at which full austenitization is achieved (Ac3) is higher than the respective theoretically predicted value (for "static" slow warm up). This effect was firstly mentioned by Leblond [16] and was integrated to the weld modelling approach by the authors of the present paper [3] based on measurements of theoretical and real Ac3 found in [18]. During cooling down, the selection of material models for the austenitized proportion in each area of the weld, is based on predictions of the transformed microstructure according to continuous cooling transformation (CCT) diagram or assessment of microstructure through measurements. The process of selecting the respective material models is presented in Fig. 2.

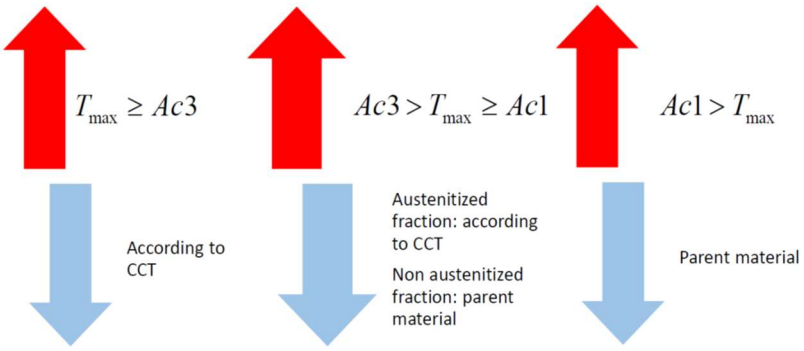

Fig. 2 Assumed microstructural transformations depending on T_{max} values [3]

The importance or negligibility of microstructural changes during modelling of ferritic or austenitic steels respectively has been confirmed in the past [3], [12]. Softening in the HAZ of aluminum alloys was as well successfully modelled in a previous study of the authors [10]. Three new models were assigned during cooling down, one of fully recrystallized material in the FZ and two of partially recrystallized microstructure in the HAZ (different levels of recrystallization). Nevertheless, a quantification of this influence on WRS is not known to the authors of the present study. The same problem arises as well when high strength steels are regarded. Liu et al. [19] and Lee and Chang [20] simulated weldments of ASTM A514 (yield strength of 717 MPa) with phase changes and a high strength carbon steel with yield strength of 790 MPa by neglecting them respectively.

However, the present approach has not yet been extended to the simulation of multi-pass welds. Material that lies within the boundaries of a single pass is being influenced from the subsequent weld passes. Therefore, a single consideration of T_{max} and t_{85} during the thermal cycle of the preceding weld pass is not sufficient for modelling precisely the material behavior after completion of the consecutive pass. Previous studies regarding simulation of multi-pass welds, which are known to the authors of the present paper, have been carried out either for cases, whereby phase transformations were negligible ([21], [22], [23], [24], [25]) or the validation of the applied models for multi-pass welding was carried out based on CCT diagrams ([26], [6]). In the latter case, special consideration has to be made, in order to properly model the influence of multi-pass welds, as CCT diagrams describe only the influence of a single thermal cycle on the parent material.

Modelling of mechanical behaviour

During modelling of the mechanical field, the nodal temperature history from the prior transient thermal analysis is applied as body force nodal loads (thermal strains ε_{th}), which are calculated based on the temperature dependent coefficient of thermal expansion α^{se} [15]

$$\varepsilon^{th} = a^{se}(T) \cdot (T - T_{ref}) \ . \tag{6}$$

Solution takes place in a quasi-static structural analysis, whereby temperature dependent material parameters and the restraints applied to the real welded component are modelled [3]. Quasi-static structural analysis is governed by the following equation:

$$f_s(u) - p(t) = 0 \ . \tag{7}$$

Usually, components are clamped down during welding. Fixing of the respective nodes in the FE models is a common approach of modelling but deviates from physical restraining reality. An alternative approach applied elsewhere [9] is the use of linear spring elements, restraining the respective nodes (see Fig. 4). The free edge of the spring is then fixed parallel to its length direction. Therewith, only very small displacements are allowed, which coincides with the situation in real "clamping".

In most cases, mechanical solution is based on classical theory of strain-rate independent plasticity [27]. Total mechanical strain is decomposed to elastic and plastic parts (Eqn. (8)).

$$\varepsilon_{tot}^{mech} = \varepsilon_{el} + \varepsilon_{pl} \ . \tag{8}$$

The stress σ is proportional to the elastic strain ε_{el} according to Hooke's law for linear isotropic material behaviour, which is presented in terms of Young's modulus and Poisson's ratio and in index notation in the following equation (Eqn. (9)),

$$\varepsilon_{ij} = \frac{1}{E}(\sigma_{ij} - v(\sigma_{kk}\delta_{ij} - \sigma_{ij})), \tag{9}$$

where δ_{ij} is the Kronecker delta. Von Mises yield criterion (Eqn. (10)

$$f(\sigma, \sigma_y) = \sigma_e - \sigma_y = 0, \tag{10}$$

is widely applied for metallic materials, where σ_ε is the von Misses effective stress

$$\sigma_e = \sqrt{\frac{3}{2}\left(\sigma : s - \frac{1}{3}tr(\sigma)^2\right)} \ . \tag{11}$$

Isotropic hardening is usually applied, during welding simulations, as theoretically, heating the material up to near melting temperature erases previous hardening history and the material deforms as virgin [23], [28]. Nevertheless, kinematic hardening provided better results elsewhere [9], [12]. In some cases, even mixed hardening models are proposed [28].

Lindgren [8] proposed that during weld simulation, when very high accuracy is required, strain-rate dependent plasticity should be considered, without providing though any information regarding the order of magnitude of the influence on calculated WRS. Previous analyses of the authors of the present paper have showed that in the heat affected zone (HAZ) and the fusion zone (FZ) of a 3-pass butt-weld, strain rates of up to 0.122 s^{-1} are present [11]. Although this value lies clearly lower than the classical dynamic cases such as modelling of ballistic tests or car crash simulation (100 s^{-1}), still clearly deviates from the static case ($\dot{\varepsilon} \rightarrow 0$). Several models have been proposed in the past for modelling of the strain-rate dependent behavior of steel. The following model proposed by Perzyna in 1966 [29] is appropriate for implicit FE simulations like in the present case (Eqn. 12)

$$\dot{\bar{\varepsilon}}_{pl} = \gamma \left(\frac{\sigma}{\sigma_0} - 1 \right)^{1/m} . \tag{12}$$

REVIEWING THE INLUEFNCE OF INPUT PARAMETERS

Results from previous and new FE analyses, which were all carried out according to the above-described theoretical background, are presented in the current study in order to review specific aspects of weld simulation. FE commercial software ANSYS [15] was applied in all cases. Solid 8 node elements "solid 90" and "solid 180" were applied for the transient thermal and the static structural analyses respectively in all cases. Mesh element dimensions were 0.4 mm x 0.4 mm x 5 mm (width x height x length) in the FZ and the HAZ in all cases. The following aspects were investigated:

A: MODELLING OF MECHANICAL BOUNDARY CONDITIONS (BC)

A single-pass weld component of Swedish steel HT36 (equivalent to S355) with dimensions of 2000 mm x 1000 mm x 15 mm was simulated in [9] (component A in the present study). Geometry of the weld section is presented in Fig. 3. The component was welded with submerged-arc welding (three electrodes welding consecutively), an electric power of 98 kW and a welding speed of 25 mm/s (150 cm/min; 3.92 kJ/mm heat input). Applied material parameters are given in [3]. Clampers were modelled either by fixing the respective nodes in all directions or by applying linear spring elements with stiffness of 10^6 N/mm to all nodes in the clamped area in the longitudinal and transverse direction and fixing their vertical displacement. The results are compared with measurements for an identical component found elsewhere [2].

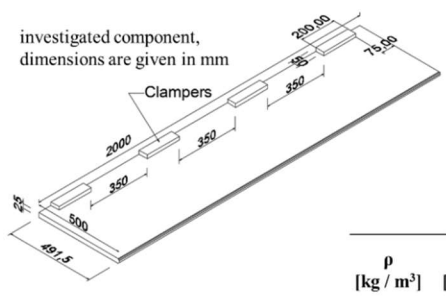

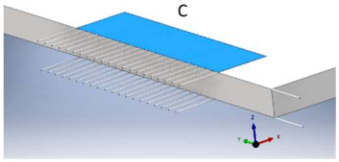

spring element setup for simulating clampers

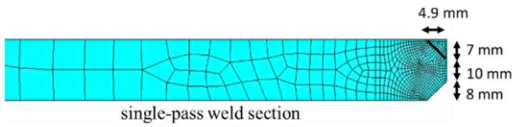

single-pass weld section and the respective mesh

material properties of investigated HT36

ρ [kg / m³]	T [°C]	c [kJ / (kg · °C)]	K [W / (m · °C)]	Yield Strength [MPa]	Young's Modulus [GPa]	Tangent Modulus [GPa]
7800	0	0,4	40	355	220	2,2
	200	0,5	40	320	200	0
	600	0,6	40	102	131	0
	700	0,9	36	84	98	0
	850	1,3	26	56	49	0
	900	0,6	26	47	32	0
	1500	0,8	33	5	0	0

Fig. 3 Investigated component A

B: THERMAL INPUT AND WELDING SEQUENCE OF MULTI-PASS WELDS

Influence on the WRS, which can be caused by possible erroneous modelling of thermal heat input is investigated in [12]. The 5-pass X-grooved butt-weld with dimensions 300 mm x 300 mm x 10 mm by AISI 316L, which is presented in Fig. 4, was simulated (component B in the present study) and different cases of differentiating heat input were modelled. The component was initially considered to be welded with an electric power of 4.3 kW, a welding speed of 5 mm/s (30 cm/min; 0.86 kJ/mm heat input) and the welding sequence A-B-C-D-E. Applied material parameters are given in [13]. Heat input was changed by either increasing the welding speed, or reducing the energy input rate (see respective Table of Fig. 4). The results are reviewed from a different scope in the present study in order to estimate the possible error of calculated WRS under the assumption that an under- or overestimation of ± 10 % of the weld heat source's efficiency has taken place.

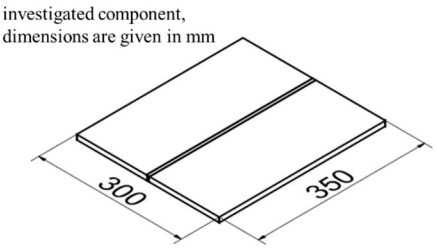

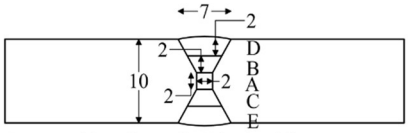

5-pass weld section and original welding sequence, dimensions are given in mm

material properties of AISI 316L

T [°C]	K [W / (m K)]	C [kJ / (kg K)]	ρ [kg / m³]	α x 10⁶ [-]	Young's Modulus [GPa]	ν [-]
20	13,3	0,47	7966	15,2	195	0,267
400	19,4	0,55	7814	17,4	172	0,322
1000	27,5	0,676	7535	19,3	100	0,229
1420	31,9	0,765	7320	20,7	10	0,223
1460	320	0,765	7320	20,7	2	0,223
3000	320	0,765	7320	20,7	2	0,223

reviewed investigated cases found in [9]

Model	Investigated variable
H1	initial welding parameters
V1	welding speed – 25 % reduced
V2	welding speed – 50 % reduced
Q1	energy input rate – 25 % increased
Q2	energy input rate – 50 % increased

Fig. 4 Investigated component B

C: INFLUENCE OF MICROSTRUCTURAL CHANGES IN ALUMINIUM WELDING

Previous numerical studies regarding welding of Aluminum alloy initially presented at [10], were repeated in the present study and in [30], by neglecting this time the metallurgical transformations, in order to evaluate qualitatively and quantitatively the influence of recrystallization in the HAZ of aluminum alloys on the simulated WRS. The single-pass V grooved component of EN AW-6060 with dimensions 300 mm x 300 mm x 5 mm, welded with an electric power of 3.1 kW and a welding speed of 10 mm/s (60 cm/min; 0.31 kJ/mm heat input), which is presented in Fig. 5 is modelled.

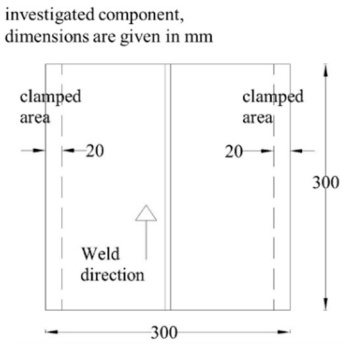

material properties of EN AW 6060

Temperature [°C]	c [J/(kg K)]	K [W/(m K)]	Yield Strength [MPa]	Yield Strength (HAZ) [Mpa]
20	911	192	140	60
100	944	197	127	54,6
400	1067	218	9,7	4,3
655	1172	236	1	1
1000	1313	260		
1590	1555	301		
5000	2953	540		

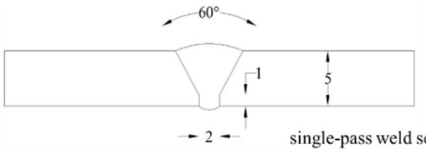

single-pass weld section, dimensions are given in mm

Fig. 5 Investigated component C

D: STRAIN-RATE DEPENDENCY OF WELDING RESIDUAL STRESSES

Numerical studies regarding single-pass butt-welding of a S355 component (component D) with dimensions 500 x 200 x 5, whose section and respective FE model is shown in Fig. 6, were repeated in [11], by taking into consideration this time the strain-rate dependency of the investigated material. Goal was the qualitative and quantitative evaluation the influence of strain-rate dependency on the simulated WRS. A single-pass V grooved component welded with an electric power of 7.934 kW and a welding speed of 6.7 mm/s (40 cm/min; 1.18 kJ/mm heat input) is modelled. Three different cases were considered, one strain-rate independent (BC) and two strain-rate dependent cases VA_TM1 and VA_TM2, whereby the strain-rate dependent material behavior was calibrated based on material data found in [31] and [32], [33] and [34] respectively.

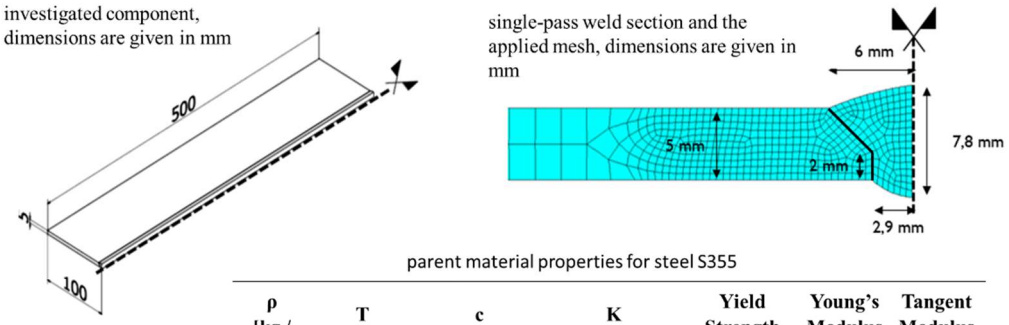

parent material properties for steel S355

ρ [kg / m³]	T [°C]	c [kJ / (kg · K)]	K [W / (m · K)]	Yield Strength [MPa]	Young's Modulus [GPa]	Tangent Modulus [GPa]
7800	0	0.4	40	355	210	2.2
	200	0.5	40	355	210	2.2
	600	0.6	40	177	131	2.2
	700	0.9	36	134	98	2.2
	850	1.3	26	69	49	0
	900	0.6	26	47	32	0
	1500	0.8	33	5	0	0

Fig. 6 Weld section and the applied FE mesh for component D

A PROPOSAL FOR THE EXTENSION OF THE PRESENT MODEL TO MULTI-PASS WELDING AND HIGH STRENGTH STEELS

The present approach, as mentioned-above, is based on the use of CCT diagrams in order to predict the transformed microstructure after cooling-down of a single-pass butt-weld [3]. CCT diagrams have already been used for calibration of algorithms, which were applied for the simulation of multi-pass welds ([26], [6]). Nevertheless, extra aspects have to be considered so that the effect of consecutive passes to the microstructure of preceding passes can be caught by such an approach, as the CCT diagrams describe a single thermal cycle. In both of these cases there was a non negligible deviation between measured and simulated WRS, especially in the longitudinal direction (almost 200 MPa for [6], even higher for [26]). Moreover, in the case of high strength steels, CCT diagrams are usually not available

in literature although the research interest on these materials is increasing in the last years (see [35]).

With the present approach, in the case, whereby a CCT diagram is available, it can be assumed that succeeding weld passes carry on the austenitization of the boundary areas of previous passes, if there was no full austenitization, or that there is a reaustenitization of the previously fully-austenitized materials. In both cases it can be assumed as well that the investigated material's cooling down behaviour still can be described by the CCT diagram of the parent material despite the thermal treatment of the preceding passes.

An alternative approach would be the use of hardness measurements on the macro sections of welded components. This measurements could be applied either as a validation of the modelling approach based on the CCT diagrams validating the above-mentioned assignments or as direct input for the material behaviour of various areas of the weld section. The relation of hardness and yield strength of steel has been proven in several cases in the past and various equations have been proposed such as in [36] and [37]. Moreover, the hardness of the individual steel phases at room temperature as a function of the chemical composition can be analytically calculated [38]. Knowing the proportion of the metallurgical phases and the yield strength and hardness, it could be possible to calculate the proportion of phases at each area of the macro section based on the hardness measurements.

RESULTS AND DISCUSSION

The calculated longitudinal WRS for the HT36 component A are presented in Fig. 6. "Meas." stands for measured WRS found in [2], while "Fixed" and "Springs" are referring to the respective applied modelling approach of BC. In both cases, tensile longitudinal stresses, higher than the nominal yield limit of the material at room temperature are met in the FZ and HAZ and compressive stresses in the areas away from the weld. In the case of modelling with spring elements, tensile stresses of even up to 700 MPa are met (yield strength in the weld area is higher than the nominal 355 MPa due to the phase changes taken place – increase of bainitic and martensitic phases), while for the fixed case the maximum tensile stress is not higher than 450 MPa. Although both approaches produce similar results qualitatively, the agreement of the spring model with the measurements inside the weld section is clearly better. Similar improvement due to use of spring elements was observed as well in the case of calculated transverse WRS [9]. Nevertheless, it seems that initial expectations that the fixed model, being stiffer, would produce higher WRS are not met. However, significant bending of the plate takes place and the interpretation of the results based on the simplified theoretical expectations is not valid anymore, as the profile stresses of Fig. 6 are measured on top surface of the plate. A more complex interpretation of the results taking into consideration the 3D effects should be made.

The calculated longitudinal WRS for the AISI 316L component B are presented in Fig. 7. Similar profiles of longitudinal WRS are calculated in all investigated cases (see Table 1). Tensile and compressive WRS are met near and away from the weld respectively. The increase of the heat input, either by increase of thermal power or reduction of welding speed, shifts down the calculated profile of WRS. Nevertheless, the largest deviation from the initial profile (H1) is met in the case of reduced welding speed down to 50 % (case V2),

which equals to an increase of heat input up to 100%. A difference of up to 150 MPa or 28 % between the peak tensile stresses of those two cases is observed. Similar but not so significant differentiation of the transverse WRS profiles was observed as well [13].

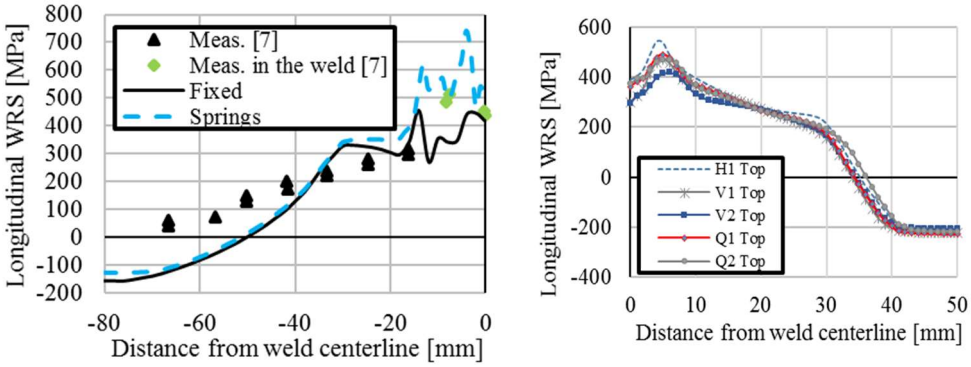

Fig. 7 Longitudinal WRS – left: Component A (HT36) – right: Component B (316L), resulting WRS on the top of the component, for the investigated cases presented in Table 1

The calculated WRS for the EN AW 6060 component C are presented in Fig. 5 for the cases of taking into consideration and neglecting the recrystallization in the HAZ. In the case of the longitudinal WRS the calculated profile differs significantly, both qualitatively and quantitatively, near the weld. Neglecting the microstructural changes, leads to a lower calculated peak stress and a shift of this peak stress from the boundaries between HAZ and parent material in the middle of the component. The second peak stress met at the left part of the WRS profile, lies on the boundaries of the clamped area of the component. Stress increase is due to fixing of the respective nodes. In the case of the transverse WRS, neglecting recrystallization causes a shift up of the calculated profile of up to 100 MPa.

The calculated longitudinal and transverse WRS for the strain-rate independent and dependent cases are presented in Fig. 9 and Fig. 10 respectively. The rate independent investigated case BC exhibits very good agreement with the measured WRS. A significant deviation is observed only inside the weld section, a region where the robustness of measured WRS is questionable, due to technical reasons. The profiles from both rate dependent investigated cases are almost identical with each other but deviate significantly from the BC case, i.e. the rate-independent model. Regarding the profiles of the longitudinal WRS, deviations from 50 MPa up to 100 MPa between the strain-independent and the rated-dependent cases are observed at the region outside the weld section. Inside the weld section, the difference between the rate dependent and independent cases is almost negligible. Nevertheless, the rate independent model seems to exhibit slightly better agreement with the measured WRS, which in the region away from the boundaries of the weld lie between the curves of the calculated WRS from the rate independent and dependent cases. In the case of the transverse WRS, a significant difference between rate independent and dependent case was observed overall, with the largest deviation to be met at the weld toe, where a difference of 140 MPa is met. The rate independent model BC exhibited in this case an overall clearly better agreement with the measured WRS than the rate-dependent

models. Equilibrium seems not to be achieved, but this is acceptable as the presented WRS are calculated and measured on the top of the plate.

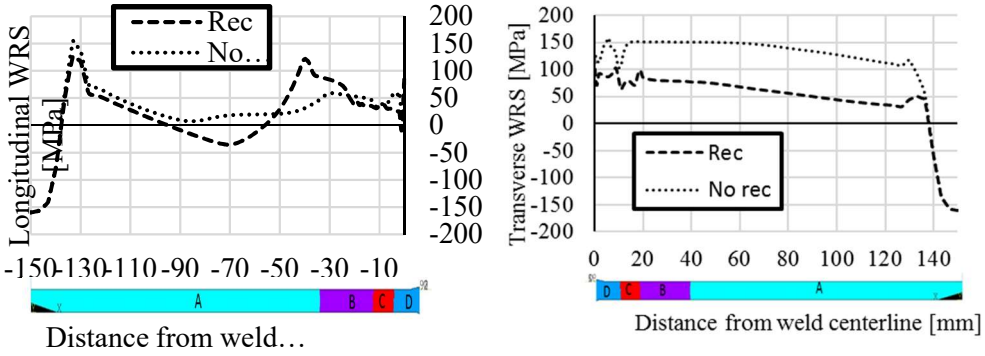

Fig. 8 WRS of the alluminum component C with and without modelling of recrystilisation in the HAZ, collored areas of the component show modelling of the microstructural changes, A: parent material, B: HAZ 50 % recrystalized, C: HAZ 100 % recrystalized, D: FZ.

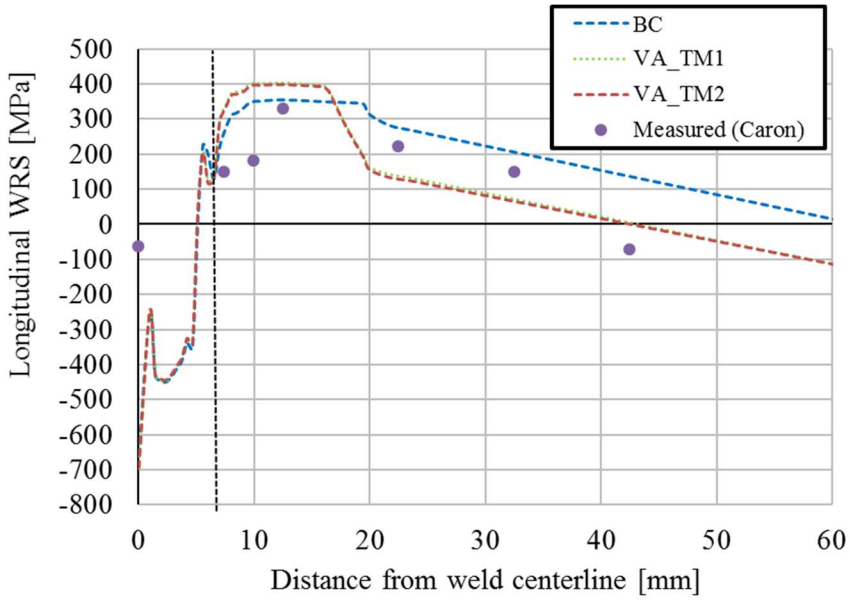

Fig. 9 Results for component D – calculated and experimentally measured longitudinal WRS on the top of the plate (measured WRS found in [6]) – vertical broken line shows the limits of the weld area [11]

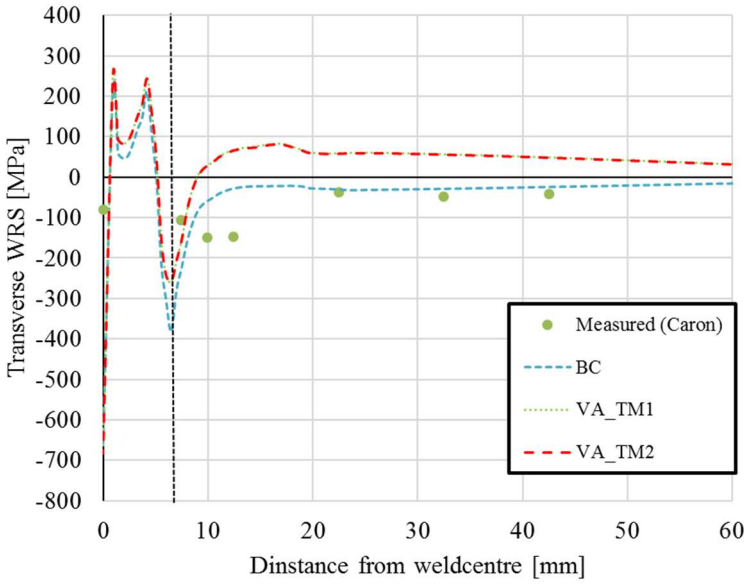

Fig. 10 Results for component D – calculated and experimentally measured transverse WRS on the top of the plate (measured WRS found in [6]) – vertical broken line shows the limits of the weld area [11]

CONCLUSIONS AND FUTURE WORK

The following conclusions were drawn, based on the above-presented results:

Applied approach for modelling of clampers during a weld simulation can have a significant effect on the calculated WRS, at least in the case of butt-welds. The use of spring elements for modelling the longitudinal and transverse restraints in the clamped area produces results that show better agreement with experimentally measured WRS. Moreover, as higher tensile WRS are calculated, this approach lies on the safe side. This modelling approach is therefore suggested for adoption in practical applications as well.

A possible erroneous modelling of the weld heat source could lead to an underestimation of the WRS and therefore non-conservative results. An increase of 100 % of the heat input led to a reduction of 28 % of the peak tensile stress (worst case scenario). Assuming a linear behavior, an overestimation of 10 % of the heat source coefficient would lead to an underestimation of 2.8 % of the peak tensile stresses. This deviation lies in the boundaries of the acceptable numerical error, of practical weld simulations (± 10 % [3]). Therefore, applying values for the weld metal arc efficiency from literature or previous measurements during the simulation of WRS, is considered valid.

Aluminum welding simulations neglecting the recrystallization in the HAZ, produce erroneous results. A lower longitudinal peak stress is calculated and is present at the middle of the component. Simulations considering the microstructural changes show that the peak stress is met on the boundaries of the HAZ, exhibiting a much more crucial case, regarding fatigue strength of the investigated component. Therefore, neglecting recrystallization in

the HAZ of aluminum weld during weld simulation is not conservative and should be avoided.

Applying strain rate dependent material models during a weld simulation produces significant deviation in the profiles of calculated WRS in comparison with the classical static material models. A deviation of up to 150 MPa was observed in the present case between rate independent and dependent cases. Therefore, strain rate dependency cannot be neglected during weld simulation when high accuracy is required. Nevertheless, the strain-rate independent case provided results with better agreement in the case of transverse WRS and this incompatibility has to be clarified.

The present method has been proven to provide accurate results with less computational effort and increased simplicity in comparison with previous modeling approaches for single pass-welds [3]. A validation of the above-mentioned extension for the case of multi-pass welds and high strength steels is therefore dictated. Comparison with measured WRS of real multi-pass welds has to be carried out and the effectiveness should be compared with other approaches [26], [6].

ACKNOWLEDGEMENTS

The above presented work was carried out as a part of the framework of [39].

REFERENCES

[1] J. H. ARGYRIS, J. SJIMMAT AND K. J. WILLAM: 'Computational Aspects of Welding Stress Analysis', *Computer Methods in Applied Mechanics and Engineering*, Vol. 33, No. 1-3, pp. 635-665, 1982.

[2] B. ANDERSSON: 'Thermal Stresses in a Submerged-Arc Welded Joint Considering Phase Transformations', *Trans. ASME,* Vol. 100, pp. 356-362, 1978.

[3] P. KNOEDEL, S. GKATZOGIANNIS AND T. UMMENHOFER: 'Practical Aspects of Welding Residual Stress Simulation', *Journal of Constructional Steel Research*, Vol. 132, pp. 83-96, 2017.

[4] P. DONG: 'Residual Stress Analyses of a Multi-Pass Girth Weld: 3-D Special Shell Versus Axisymmetric Models'*, Journal of Pressure Vessel Technology,* Vol. 123, No. 2, pp. 207-213, 2001.

[5] D. DENG AND H. MURAKAWA: 'Numerical simulation of temperature field and residual stress in multi-pass welds in stainless steel pipe and comparison with experimental measurements'*, Computational Materials Science,* Vol. 37, pp. 269-277, 2006.

[6] C. HEINZE, C. SCHWENK, M. RETHMEIER AND J. CARON: 'Numerical Sensitivity Analysis of Welding-Induced Residual Stress Depending on Variations in Continuous Cooling Transformation Behavior'*, Front. Mater. Sci.,* Vol. 5, No. 2, pp. 168-178, 2011.

[7] A. A. BHATTI, Z. BARSOUM, H. MURAKAWA AND I. BARSOUM: 'Influence of Thermo-Mechanical Material Properties of Different Steel Grades on Welding Residual Stresses and Angular Distortion'*, Materials and Design,* Vol. 65, pp. 878-889, 2015.

[8] L. E. LINDGREN: *Computational Welding Mechanics – Thermomechanical and Microstructural Simulations*, 1st Edition, Woodhead Publishing, Cambridge, England, 2007.

[9] S. GKATZOGIANNIS, P. KNOEDEL AND T. UMMENHOFER: 'FE Welding Residual Stress Simulation – Influence of Boundary Conditions and Material Models', *EUROSTEEL 2017, September 13–15, 2017, Copenhagen, Denmark, Ernst & Sohn, CE/papers,* 2017.

[10] P. KNOEDEL, S. GKATZOGIANNIS AND T. UMMENHOFER: 'FE Simulation of Residual Welding Stresses: Aluminum and Steel Structural Components', *Key Engineering Materials*, Vol. 710, pp. 268-274, 2016.
[11] S. GKATZOGIANNIS, P. KNOEDEL AND T. UMMENHOFER: 'Strain-Rate Dependency of Simulated Welding Residual Stresses', *Journal of Material Performance and Engineering*, 2017.
[12] S. GKATZOGIANNIS, P. KNOEDEL AND T. UMMENHOFER: 'Influence of Welding Parameters on the Welding Residual Stresses', *Proceedings of the VII International Conference on Coupled Problems in Science and Engineering, Rhodes Island, Greece, June 12 – 14*, pp. 767-778, 2017.
[13] J. A. GOLDAK, A. CHAKRAVARTI AND M. BIBBY: 'A New Finite Element Model for Welding Heat Sources', *Metall. Trans. B,* Vol. 15, pp. 299-305, 1984.
[14] J. N. DUPONT AND A. R. MARDER: 'Thermal Efficiency of Arc Welding Processes', *Weld. J.*, pp. 406-416, 1995.
[15] ANSYS® Academic Research, Release 18.2, Help System, ANSYS, Inc., 2018.
[16] J. B. LEBLOND AND J. DEVAUX: 'A New Kinetic Model for Anisothermal Metallurgical Transformations in Steels including Effect of Austenite Grain Size', *ACTA Metall.*, Vol. 32, pp. 137-146, 1984.
[17] D. P. KOISTINEN AND R. E. MARBURGER: 'A General Equation Prescribing the Extent of the Austenite-Martensite', *ACTA Metall.*, Vol. 7, pp. 59-61, 1959.
[18] M. Q. MACEDO, A. B. COTA AND F. G. DA S. ARAÚJO: 'The Kinetics of Austenite Formation at High Heating Rates', *Metal. E Mater.*, Vol. 64, pp. 163-167, 2011.
[19] W. LIU, J. MA, F. KONG, S. LIU AND R. KOVACEVIC: 'Numerical Modeling and Experimental Verification of Residual Stress in Autogenous Laser Welding of High-Strength Steel', *Lasers Manuf. Mater. Process. 2,* pp. 24-42, 2015.
[20] C. H. LEE AND K .H. CHANG: 'Prediction of Residual Stresses in High Strength Carbon Steel Pipe Weld Considering Solid-State Phase Transformation Effects', *Computers and Structures,* Vol. 89, pp. 256-265, 2015.
[21] B. BRICKSTAD AND B. L. JOSEFSON: 'A Parametric Study of Residual Stresses in Multi-Pass Butt-Welded Stainless Steel Pipes', *International Journal of Pressure Vessels and Piping,* Vol. 75, pp. 11-25, 1998.
[22] D. E. KATSAREAS, C. OHMS AND A. G. YOUTSOS: 'Finite Element Simulation of Welding in Pipes: A Sensitivity Analysis', *Proceedings of a Special Symposium held within the 16th European Conference of Fracture - ECF16, Alexandroupolis, Greece, 3-7 July, 2006,* pp. 15-26, 2006.
[23] H. WOHLFAHRT, T. NITSCHKE-PAGEL, K. DILGER, D. SIEGELE, M. BRAND, J. SAKKIETTIBUTRA AND T. LOOSE: 'Residual Stress Calculations and Measurements - Review and Assessment of the IIR Round Robin Results', *Welding in the World,* Vol. 56, pp. 120-140, 2012.
[24] S. NAKHODOCHI, A. SHOKUFAR, S. A. IRAJ AND B. G. THOMAS: 'Residual Stress Calculations and Measurments- Review and Assessment of the IIR Round Robin Results', *Journal of Pressure Vessel Technology, Vol*. 137, 2015.
[25] C. K. LEE, S. P. CHIEW AND J. JIANG: '3D Residual Stress Modelling of Welded High Strength Steel Plate-to-Plate Joints', *Journal of Constructional Steel Research,* Vol. 84, pp. 94-104, 2013.
[26] L. BÖRJESSON AND L. E. LINDGREN: 'Simulation of Multipass Welding With Simultaneous Computation of Material Properties', *Journal of Engineering Materials and Technology,* Vol. 123, pp. 106-111, 2001.
[27] J. LUBLINER: 'Plasticity Theory', Dover Publications, 3d Edition, New York, USA, 2008.
[28] J. MULLINS AND J. GUNNARS: 'Influence of Hardening Model on Weld Residual Stress Distribution', *Research Report 2009:16, Inspecta Technology AB,* Stockholm, Sweden, 2009.

[29] P. PERZYNA: 'Fundamental Problems in Viscoplasticity', *Advances in Applied Mechanics,* Vol. 5, pp. 243-377, 1966.
[30] S. GKATZOGIANNIS, P. KNOEDEL AND T. UMMENHOFER: 'Reviewing the Influence of Welding Setup on FE-simulated Welding Residual Stresses', *Proceedings of the 10th European Conference on Residual Stresses - ECRS10, Leuven, Belgium, on 11-14 September, 2018.*, accepted for publication.
[31] N. JONES: *Structural Impact,* 2nd Edition, Cambridge University Press, New York, USA, 2012.
[32] D. FORNI, B. CHIAIA AND E. CADONI: 'Strain Rate Behaviour in Tension of S355 Steel: Base for progressive collapse analysis', *Engineering Strcutrures,* Vol. 119, pp. 167-173, 2016.
[33] M. KNOBLOCH, J. PAULI, M. FONTANA: 'Influence of The Strain Rate on the Mechanical Properties of Mild Carbon Steel at Elevated Temperatures', *Materials and Design,* Vol. 49, pp. 553-565, 2013.
[34] D. FORNI, B. CHIAIA AND E. CADONI: 'High Strain Rate Response of S355 at High Temperatures', *Materials and Design,* Vol. 94, pp. 467-478, 2016.
[35] J. SCHUBNEL, S. GKATZOGIANNIS, M. FARAJIAN, P. KNOEDEL, T. LUKE AND T. UMMENHOFER: '*Rechnergestütztes Bewertungstool zum Nachweis der Lebensdauerverlängerung von mit dem Hochfrequenz-Hämmerverfahren (HFMI) behandelten Schweißverbindungen aus hochfesten Stählen',* Research Project DVS 09069 – IGF 19227 N, 2018 (in progress).
[36] E. J. PAVLINA AND C.J. VAN TYNE: 'Correlation of Yield Strength and Tensile Strength with Hardness for Steels', *Journal of Materials Engineering and Performance,* Vol. 17, No. 6, pp. 888-893, 2008.
[37] P. ZHANG, S. X. LI AND Z. F. ZHANG: 'General Relationship Between Strength and Hardness', *Materials Science and Engineering A,* Vol. 529, No. 6, pp. 62-73, 2011.
[38] J. HILDEBRAND: '*Numerische Schweißsimulation: Bestimmung von Temperatur, Gefüge und Eigenspannung an Schweißverbindungen aus Stahl- und Glaswerkstoffen',* Dissertation, Bauhaus-Universität Weimar, 2008.
[39] S. GKATZOGIANNIS: '*Finite Element Simulation of High Frequency Hammer Peening',* Doctoral Thesis , KIT, Karlsruhe Institute of Technology, 2018 (in progress).